# Synthesis, microstructure, magnetic properties and Raman scattering of single-crystalline $BiFeO_3$ nanorods prepared by hydrothermal technique

YU DENG[a,b,*], DI WU[b], QIANG CHEN[a], YOUWEI DU[b]
[a]*Center for Modern Analysis, Nanjing University, Nanjing 210093, China*
[b]*Nanjing National Laboratory of Microstructures, Nanjing University, Nanjing 210093, China*

$BiFeO_3$ (BFO) is an attractive material for multifunctional devices. Besides good ferroelectricity and magnetism, BFO also shows large coupling responses and high photo-catalysis efficiency at room temperature (RT). To study the magnetic and phonon properties in BFO nanostructures, we prepared single-crystalline BFO nanorods with diameters of 15-40 nm and lengths of 100-400 nm by hydrothermal technique. XRD, TEM, EDX, SQUID and Raman scattering were used to investigate the samples. The BFO nanorods exhibit a rhombohedra phase and grow along the [110] crystallographic direction. Owing to the small size, enhanced spin-glass-type magnetism was detected in the BFO nanorods under RT. Between 77 K and 120 K, a large phonon abnormality associated with the spin-two-phonon coupling was revealed by Raman scattering. With emphasis on the size effects, the microstructural, magnetic and phonon properties of the BFO nanorods have also been discussed.

(Received February 10, 2012; accepted April 11, 2012)

*Keywords:* Nanorods, Microstructure, Magnetic property, Laser Raman scattering, Hydrothermal

## 1. Introduction

Recently, multiferroic BFO has become more and more attractive due to its potential applications in the memories, photo-catalysts, and magnetoelectric devices [1-7]. Particularly, BFO one dimensional nanostructures (1DNs) are of great interests because their size-dependent properties. As known, the wavelength for incommensurate cycloid spin structure in BFO is 62 nm. With diameters below 62 nm, BFO 1DNs can exhibit enhanced magnetism, large dielectric tenability and giant magnetoelectricity [1-7]. Although many efforts were focused on the BFO 1DNs and some extraordinary properties have been developed [3-5], the controllable synthesis of high-quality BFO 1DNs and the understanding of their size effects are still challenges.

In this work, we prepared single-crystalline BFO nanorods through cost-effective hydrothermal methods. The microstructure and hydrothermal growth of the nanorods were examined. An enhanced ferromagnetism was detected in the BFO nanorods at RT. The spin-glass magnetism freezing and the spin-two-phonon coupling behaviors of the BFO nanorods were also studied at low temperature.

## 2. Experimental

The BFO nanorods were synthesized by hydrothermal technique. Firstly, $Bi(NO_3)_3{\cdot}5H_2O$ and $FeCl_3{\cdot}6H_2O$ (1:1 molar ratio) were dissolved in ethylene glycol, accompanying with stirring and ultrasound vibrating. Secondly, ammonia was added into the mixed solution until the pH value reaches 10. After that, the sediments were taken out and washed with distilled water for several times. Thirdly, the sediments were added into a NaOH solution (1M) in a sealed Teflon-lined steel autoclave, stirring for 0.5h and then hydrothermally treating at 155$^{o}$C for 100h. Finally, the sediments was washed by distilled water and dried at 80 $^{o}$C to get the BFO nanorods. For comparison analysis, BFO micrometer and nanometer structures of different sizes were also prepared by similar hydrothermal methods.

X-ray diffraction (XRD) was performed on a Rigaku D/MAX-RA diffractometer with Cu incident radiation. Two transmission electron microscopes (TEM) of JEM-2100 and Technai20, which are equipped with Energy Dispersive X-ray Spectrometers (EDX), were used for microstructural investigations. The magnetic properties were examined by a superconducting quantum interference device (SQUID) magnetometer. The samples were pressed into pellets for magnetic detections. Raman scattering was measured by a HR-800 Raman spectrometer with Linkam heating and cooling stages, using the 488 nm laser at 10 mW.

## 3. Results and discussion

Fig. 1 represents the XRD pattern of the as-prepared samples, which are well crystallized with perovskite structure [2,4]. All the diffraction lines are successfully indexed to the rhombohedra phase (R3c) BFO (JCPDS No. 71-2494). There are no impurity phases such as the $Bi_2Fe_4O_9$ or $Bi_2O_3/Fe_2O_3$. Fig. 2a and Fig. 2b show the TEM image of the BFO nanorods and the corresponding EDX spectrum, respectively. We can clearly see that the nanorods have diameters of 15-40 nm and lengths of 100-400 nm, with good stoichiometric proportion. As illustrated in Fig. 2c, we also found that the nanorods prefer to get together side-by-side, looking like thicker nanorods or nanosheets. Fig. 2d further shows the high-resolution TEM (HRTEM) image of a BFO nanorod, as well as its selected area electron diffraction (SAED) pattern in the left inset. It indicates that the nanorods are single-crystalline and grow along the [110] crystallographic direction.

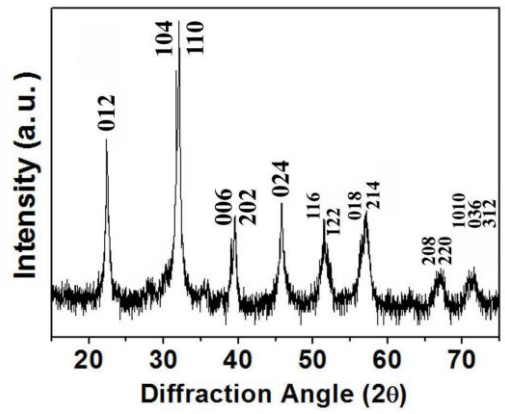


*Fig. 1. XRD pattern of the as-prepared BFO nanorods.*

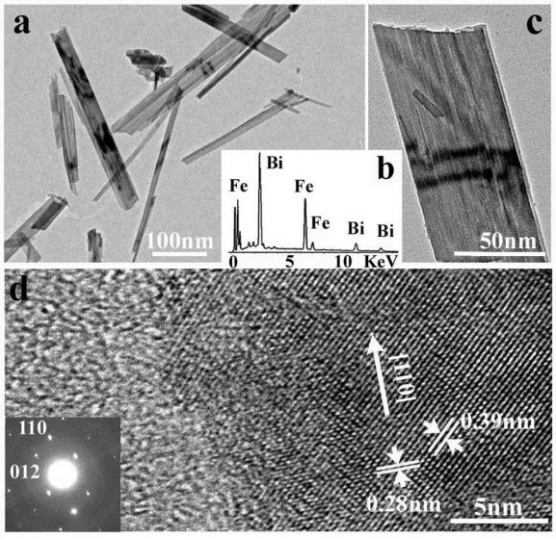


*Fig. 2. (a) TEM image and (b) EDX of the BFO nanorods, (c) TEM image for nanorods get together side-by-side, (d) HRTEM image of a BFO nanorod with the SAED pattern in left inset.*

To understand the size effects in the BFO nanorods, different-sized BFO hydrothermal products for comparison analysis were prepared through similar hydrothermal methods. Under the same hydrothermal conditions, the reactions with different alkali additives can result in completely different products [2-5]. With 0.1M, 0.5M and 5M NaOH additives, the products are BFO nanoparticles, single-crystalline nanosheets and micrometer sheets respectively, as shown in Fig. 3a-f. If the concentration of NaOH is below 0.01M or above 10M, there will be considerable impurity phases such as $Fe(NO_3)_3$ and $Bi_2Fe_4O_9$. With 1M KOH additive, the products are polycrystalline nanospheres, as shown in Fig. 3g-h. Moreover, the initial morphology of the precursors and the reaction temperatures can also effectively influence the microstructures of the final products. It evidently indicates that the hydrothermal technique is powerful in controllably synthesizing BFO nanostructures [2-5].

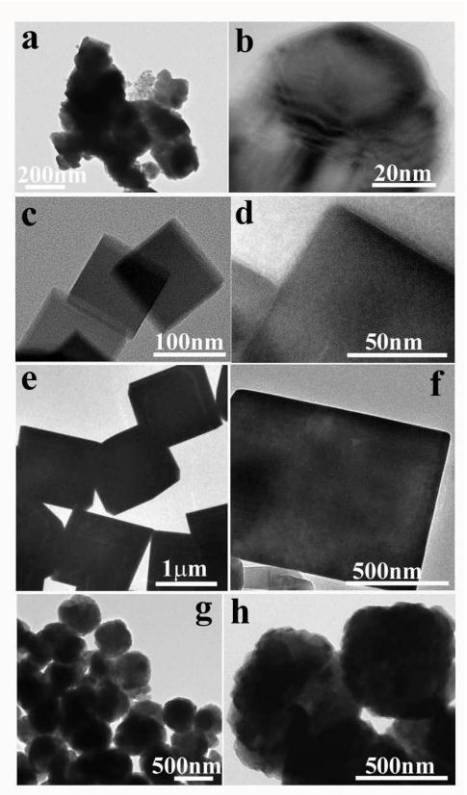


*Fig. 3. TEM and enlarged TEM images for the different hydrothermal products with the additives of (a,b) NaOH (0.1M); (c,d) NaOH (0.5M); (e,f) NaOH (5M) and (g,h) KOH (1M).*

Fig. 4a shows the magnetic hysteresis loops of the BFO nanorods at RT (300K) and 5K, respectively. We discover that the hysteresis loops are in typical ferromagnetic shape, instead of the linear antiferromagnetic one like BFO bulk crystals and ceramics [2-4, 8, 9]. As known, the ferromagnetism of BFO originates from the surface magnetic moments and is

greatly promoted by the size effects [2-6]. We attribute the RT ferromagnetism to the small size of the BFO nanorods, since their diameters are much smaller than the critical size (62 nm) to achieve large size effects [2-6]. It worth pointing out that the nanorods show a considerable RT saturated magnetism (Ms) of $0.07\mu_B$/Fe, which is comparable to the BFO thin films [8]. According to theoretical predictions, the macroscopic Ms of the BFO nanostructures can be as high as 0.11 $\mu_B$/Fe [5, 6, 10]. Our result is close to this value. For the hydrothermal products such as the BFO nanosheets and micrometer structures, the magnetic hysteresis loops have also been measured under the same conditions, showing much smaller Ms values (below 0.01 $\mu_B$/Fe). It demonstrates the size-dependent magnetic properties of the BFO nanorods. As represented in Fig. 4a, a large enhancement of ferromagnetism has been achieved in the BFO nanorods when temperature decreased to 5K. As known, at low temperature the cycloid structure of BFO becomes quite anharmonic and its negative effect on the magnetic ordering is strongly limited [4, 11]. We suggest that it is the main reason for the magnetism enhancement. Fig. 4b shows the M-T curves of the BFO nanorods. The curves are measured at H=200Oe with zero-field-cooling (ZFC) and field-cooling (FC) conditions respectively. For the ZFC curve, a cusp at 100K is observed. The cusp is the typical symbol for spin-glass type ferromagnetism and it achieves its maximum value at the blocking or freezing temperature ($T_f$) [3-6]. In our case, the $T_f$ is higher than some BFO nanoparticles and nanowires (40-90 K), evidently implying the strong size-effects in the nanorods [5, 6, 12, 13]. We know that for spin-glass-magnetic materials their ZFC and FC curves should diverge near the $T_f$ and superpose at higher temperature. It is necessary to point out that the BFO nanorods have been pressed into pellets for the magnetic measurements and the data actually represent the average of all orientations. The magnetic domains in the sample pellets could be directionally ordered to some extent under the FC condition, leading to a higher M for the FC curve than the ZFC one [4].

To further explore the size effects and the surfaces states, Raman scattering was performed on the BFO nanorods. Fig. 5a shows the Raman spectra of the BFO nanorods under different temperatures from 77 K to 700 K. At 77K, all the 13 Raman modes ($4A_1$+9E) for the rhombohedra BFO can be observed, locating between 100 $cm^{-1}$ and 800 $cm^{-1}$ [7, 14-19]. Particularly, the high-frequency lines above 1000$cm^{-1}$ are indexed as $2A_4$, $2E_8$ and $2E_9$, which are belong to the two-phonon modes introduced by the absorption edge resonance in BFO [7, 20-22]. The two-phonon modes are very sensitive to the magnetic variations in the BFO [7]. It worth pointing out that for bulk BFO materials these two-phonon Raman lines are undetectable at the exciting laser of 488 nm [7]. We have also performed the Raman scattering on the hydrothermally prepared BFO nanosheets and micrometer BFO structures, resulting in very weak two-phonon peaks. Therefore, we suggest that the intensive two-phonon lines in the BFO nanorods are strongly promoted by the size effects, which can effectively change the surface states and the absorption edge [2-4, 23, 24]. Fig. 5a clearly shows that the two-phonon band varieties with the increasing temperature, especially the dramatic variation in both intensity and shape between 77 K and 120 K. Besides the expansion and disorder induced by thermal effects, the broadening and weakening of the Raman lines are mainly caused by the variations of the magnetism [7]. Fig. 5b further shows the Gaussian fitting of the two-phonon Raman lines at 100 K and 120 K, respectively. We found that the shape changing of the two-phonon band is actually due to the relative-intensity decreasing of the $2E_8$ line. Similar to the case of Neel-temperature-transition in bulk BFO, the phonon abnormality in BFO nanorods is related to magnetism weakening [7]. The relative-intensity of the $2E_8$ is dominated by the spin-two-phonon coupling, weaker magnatism leading to weaker $E_8$ line [7, 25, 26]. Moreover, Fig. 5a shows that from 100 K to 77 K the intensity of all the two-phonon lines increases rapidly. We argue that besides the spin-phonon coupling the surface states also influence the two-phonon band, since they can change the absorption edge resonance. Therefore, the large phonon abnormal behaviors between 77 K and 120 K should be regarded as the result of both the spin-two-phonon coupling and the surface states variations.

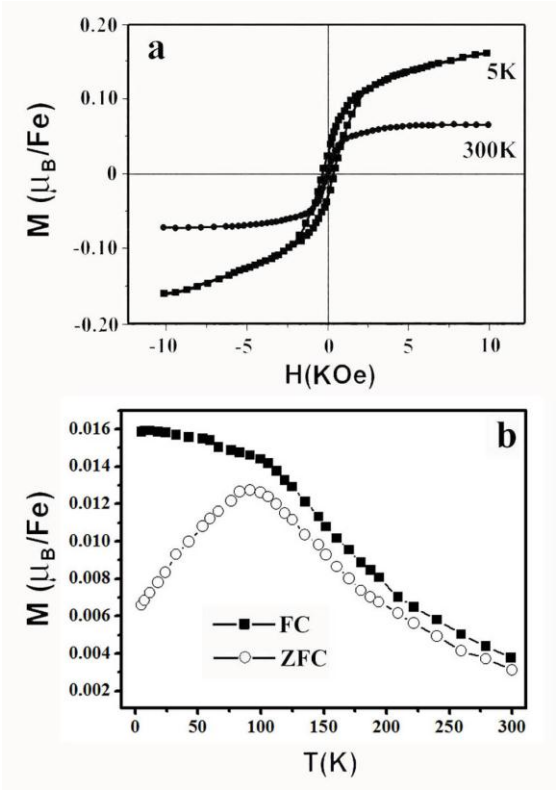


*Fig. 4. (a) Magnetic hysteresis loops of the BFO nanorods at 5K and 300K, (b) M-T curves for the BFO nanorods measured at H=200Oe under ZFC and FC conditions.*

## 4. Conclusion

In summary, we have synthesized single-crystalline BFO nanorods by hydrothermal methods. Under different temperatures, the magnetic and the phonon properties of the BFO nanorods have been studied. The microstructure and the strong size effects of the BFO nanorods were also discussed.

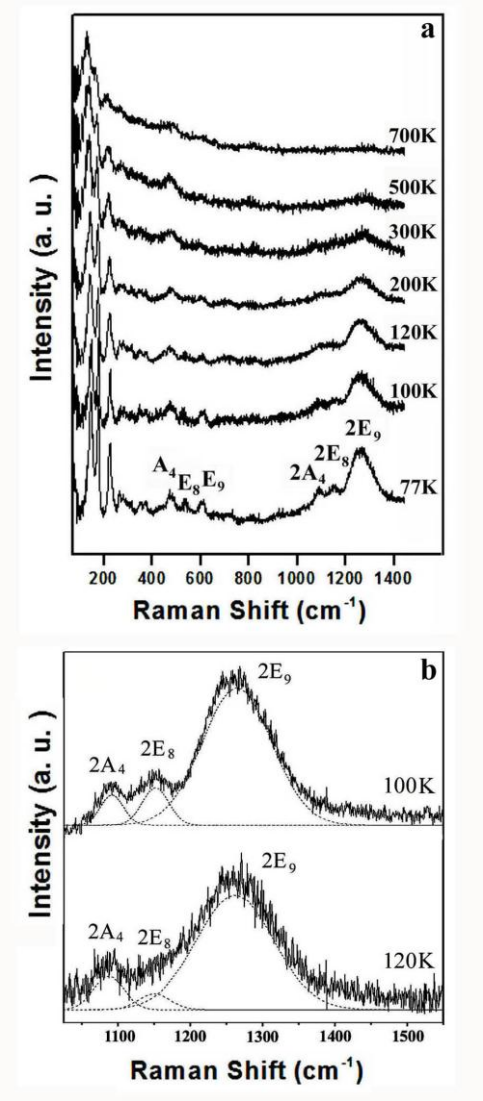


*Fig. 5. (a) Raman spectra of the BFO nanorods from 77K to 700K, (b) The Gaussian fitting for the two-phonon Raman band at 100K and 120K, respectively.*

**Acknowledgements**

This work has been supported by the National Natural Science Foundation of China No. 50802039, National Basic Research Program of China 2009CB929501, State Scholarship Fund No. 2011832411 of China scholarship council; Analysis & Test Fund, Research Fund for Young Teachers of Analysis Center and Fundamental Research Funds for the Central Universities, Nanjing University.

## References

[1] J. Wang, J. Neaton, H. Zheng et.al, Science, **299** 1719 (2003).
[2] F. Gao, X. Chen, K. Yin, S. Dong, et.al, Adv. Mater. **19**, 2889 (2007).
[3] B. Liu, B. Hu, Z. Du, Chem. Comm., **47**, 8166 (2011).
[4] F. Gao, Y. Yuan, K. Wang, et. al, Appl. Phys. Lett., **89,** 102506 (2006).
[5] T. Park, Y. Mao, S. S. Wong, Chem. Comm., **23**, 2708 (2004).
[6] T. Park, G. Papaefthymiou, A. Viescas et.al, Nano Lett., **7**, 766 (2007).
[7] M. Ramirez, M. Krishnamurthi, S. Denev et.al, Appl. Phys. Lett. **92**, 022511 (2008).
[8] W. Eerenstein, F. Morrison, J. Dho, M. Blamire, J. F. Scott, N. D. Mathur, Science **307**, 1203a (2005).
[9] S. T. Zhang, M. H. Lu, D. Wu, Y. F. Chen, N. B. Ming, Appl. Phys. Lett., **87**, 262907 (2005).
[10] C. Ederer, N. A. Spaldin, Phys. Rev. B, **71**, 224103 (2005).
[11] A. V. Zalesskii, A. K. Zvezdin, A. A. Frolov, A. A. Bush, JETP Lett. **71**, 465 (2000).
[12] L. Neel, Geophys. **5**, 99 (1949).
[13] H. Mamiya, I. Nakatani, T. Furubayashi, Phys. Rev. Lett. **80**, 177 (1998).
[14] G. L. Yuan, S. W. Or, H. L. Wa Chan, J. Appl. Phys. **101**, 064101 (2007).
[15] M. K. Singh, H. M. Jang, S. Ryu, M. Jo, Appl. Phys. Lett. **88**, 042907 (2006).
[16] M. K. Singh, S. Ryu, H. M. Jang, Phys. Rev. B **72**, 132101 (2005).
[17] P. Hermet, M. Goffinet, J. Kreisel, Ph. Ghosez, Phys. Rev. B **75**, 220102 (2007).
[18] H. Fukumura, H. Harima, K. Kisoda et al., J. Magn. Magn. Mater. **310**, e367 (2007).
[19] S. Kamba, D. Nuzhnyy, M. Savinov, et al., Phys. Rev. B **75**, 024403 (2007).
[20] K. F. McCarty, Solid State Comm. **68**, 799 (1988).
[21] T. P. Martin, R. Merlin, D. R. Huffman, M. Cardona, Solid State Comm. **22**, 565 (1977).
[22] M. J. Massey, U. Baier, R. Merlin, W. H. Weber, Phys. Rev. B **41**, 7822 (1990)
[23] A. Kumar, R. C. Rai, N. J. Podraza, Appl. Phys. Lett. **92,** 1915 (2008)
[24] V. Palkar, J. John, R. Pinto, Appl. Phys. Lett. **80**, 1628 (2002).
[25] R. Haumont, J. Kreisel, P. Bouvier, F. Hippert, Phys. Rev. B **73**, 132101 (2006).
[26] R. Haumont, J. Kreisel, P. Bouvier, Phase Transitions **79**, 1043 (2006).

*Corresponding author: dengyu@nju.edu.cn